Dust particle growth in rf silane plasmas using two-dimensional multi-pass laser light scattering

2009 New J. Phys. 11 103006

(http://iopscience.iop.org/1367-2630/11/10/103006)

New Journal of Physics
The open-access journal for physics

Dust particle growth in rf silane plasmas using two-dimensional multi-pass laser light scattering

Kil Byoung Chai[1], **C R Seon**[1,3], **S Park**[2] **and W Choe**[1,4]

[1] Department of Physics, Korea Advanced Institute of Science and Technology, 335 Gwahangno, Yuseong-gu, Daejeon 305–701, Korea
[2] Division of Physical Metrology, Korea Research Institute of Standards and Science, 209 Gajeongno, Yuseong-gu, Daejeon 305–340, Korea
E-mail: wchoe@kaist.ac.kr

New Journal of Physics **11** (2009) 103006 (8pp)
Received 26 May 2009
Published 2 October 2009
Online at http://www.njp.org/
doi:10.1088/1367-2630/11/10/103006

Abstract. We measured a spatio-temporal distribution of particle size and a spatial growth rate in a capacitively coupled silane plasma using *in situ* multi-pass laser light scattering. The two-dimensional measurement was accomplished using a low power He–Ne laser and a set of spherical mirrors across the plasma that enables us to span multiple beam paths over the plasma region in the vertical direction from the electrode sheath to the bulk plasma. In temporal, the measurement result shows two particle growth periods in which the fast particle growth (nucleation) is followed by the slow particle growth (coagulation). In spatial, the fastest particle growth occurred at the highest vertical position that corresponds to the furthest position from the sheath. The particle coagulation modeling indicates that it is consistent with the largest proto particle creation rate in the plasma bulk.

[3] Present address: National Fusion Research Institute, 113 Gwahangno, Yuseong-gu, Daejeon 305–333, Korea.
[4] Author to whom any correspondence should be addressed.

Contents

1. Introduction

Dusty plasmas are widely used in plasma processing such as plasma-enhanced chemical vapor deposition and reactive ion etching. In plasma processing, micro-particles are generated naturally by the chemical reactions between plasma species and radical species. However, the dust particles are regarded as troublemakers that bring about serious reduction of production yield and reliability [1]. In addition, in the high temperature plasma, the dust particle produced by plasma–wall interactions is a safety hazard due to its high chemical reactivity and due to the mobile tritium inventory [2]. Therefore, during the last decade, dust particle formation, growth, charging and transport have been extensively studied with various dust diagnostic methods to remove the dust particles from the plasma [3]–[6]. Among the various diagnostic methods, laser-based diagnostics have been used most frequently, because the laser diagnostics are *in situ* and non-intrusive. However, it is hard to detect the particles size as small as a few nanometers by the laser diagnostics because the scattered light intensity scales as the sixth power of the particle size. Therefore, to detect a few-nanometer-sized particle, a high power laser is necessary but this can affect the dust particles by particle evaporation or thermophoretic force [7]. Therefore, the laser diagnostic, which can measure a few-nanometer-sized particle using a low power laser, is required.

The purposes of this paper are to develop a simple, *in situ*, non-intrusive and sensitive diagnostic method for measuring the particle size in two-dimensional (2D) space and to understand the particle growth in a radio frequency (rf) silane plasma by the developed diagnostic method. We employ a multi-pass laser light scattering (LLS) method using a low power He–Ne laser, a CCD detector and a set of high reflective spherical mirrors. With little beam intensity loss, the spatio-temporal particle size is measured and the results are discussed using a coagulation model to understand the 2D characteristic of the particle growth.

2. Experimental set-up

One of the powerful methods for the *in situ* particle size measurement in plasmas is the polarization-sensitive LLS (PSLLS). The PSLLS method is based on the Lorentz–Mie scattering theory [8], which determines particle size from the ratio between the s- and the p-polarization scattering beam intensities.

In general, the 2D size measurement can be accomplished by means of a sheet laser beam spread over a measurement area [9, 10]. However, this is only possible by utilizing a high

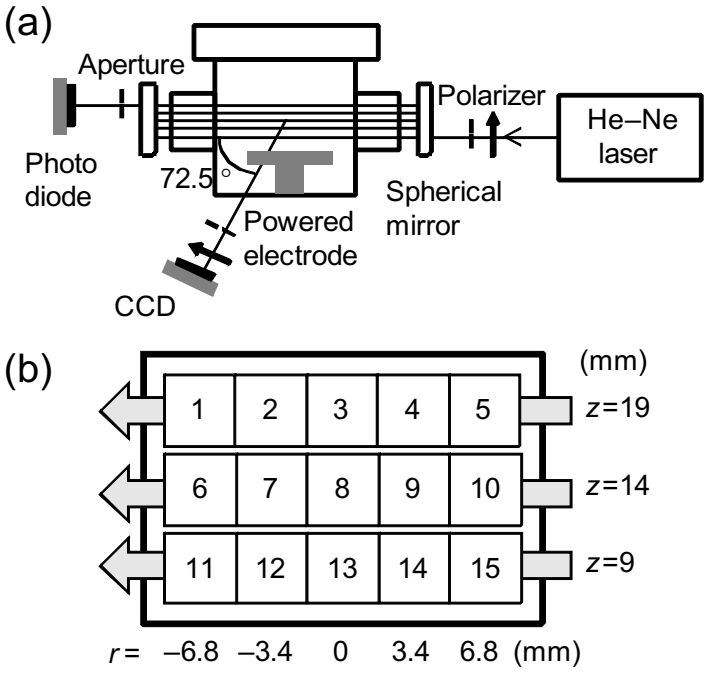

Figure 1. (a) Schematic illustration of the experimental set-up. (b) The sampling area of the CCD view inside the plasma region. The horizontal position ranges from −6.8 mm to +6.8 mm with the center corresponding to the electrode center and the vertical position is in the range of 9–19 mm above the electrode surface.

power laser to have sufficient scattered light intensity over the area. In this work, instead of using a laser sheet, 2D scattering was achieved by multiple passes of a low power (30 mW at most) He–Ne spot laser beam by means of a 2D CCD detector (768 × 494 pixels, 30 frames s^{-1}, SHC-740N, Samsung Techwin) and a set of high reflection (99.9%) spherical mirrors of 4 m focal length installed between the two chamber ports of facing each other, as illustrated in figure 1(a). In each spherical mirror, a small hole of 1 mm diameter was prepared for the spot laser beam to enter and exit. These mirrors provided five beam passes in the vertical direction inside the field view of the 15 mm × 10 mm CCD detector on which the plasma region was imaged with a lateral magnification of unity. In order to select the horizontal or vertical polarization direction of the incident and scattered beams, the directions of the two polarizers were changed simultaneously. A 632.8 nm filter was positioned in front of the CCD detector to remove unwanted light from the plasma. The scattering angle, which is the subtended angle between the incident beam and the CCD detector, was set at 72.5°. It is assumed that the index of refraction for hydrogenated amorphous silicon dust particle is 4.47 + 1.12j [11]. The distance between the detecting area inside the plasma and the CCD detector was fixed at 40 cm and an aperture with 3 mm diameter was placed in front of the CCD, resulting in a solid angle of 10^{-5}sr of the detection system. A photodiode was used to correct the ratio of each polarized incident beam. Figure 1(b) illustrates the sampling area of the CCD detector, which is the same as the sampled plasma area. Among the five laser beam passes, the first, third and fifth passes, which correspond to 72.5° scattering angle, were selected. The other two were ignored because of their weak scattering intensity with the scattering angle of 107.5°. The selected three vertical positions were 9, 14 and 19 mm above the bottom electrode surface, respectively. Each CCD

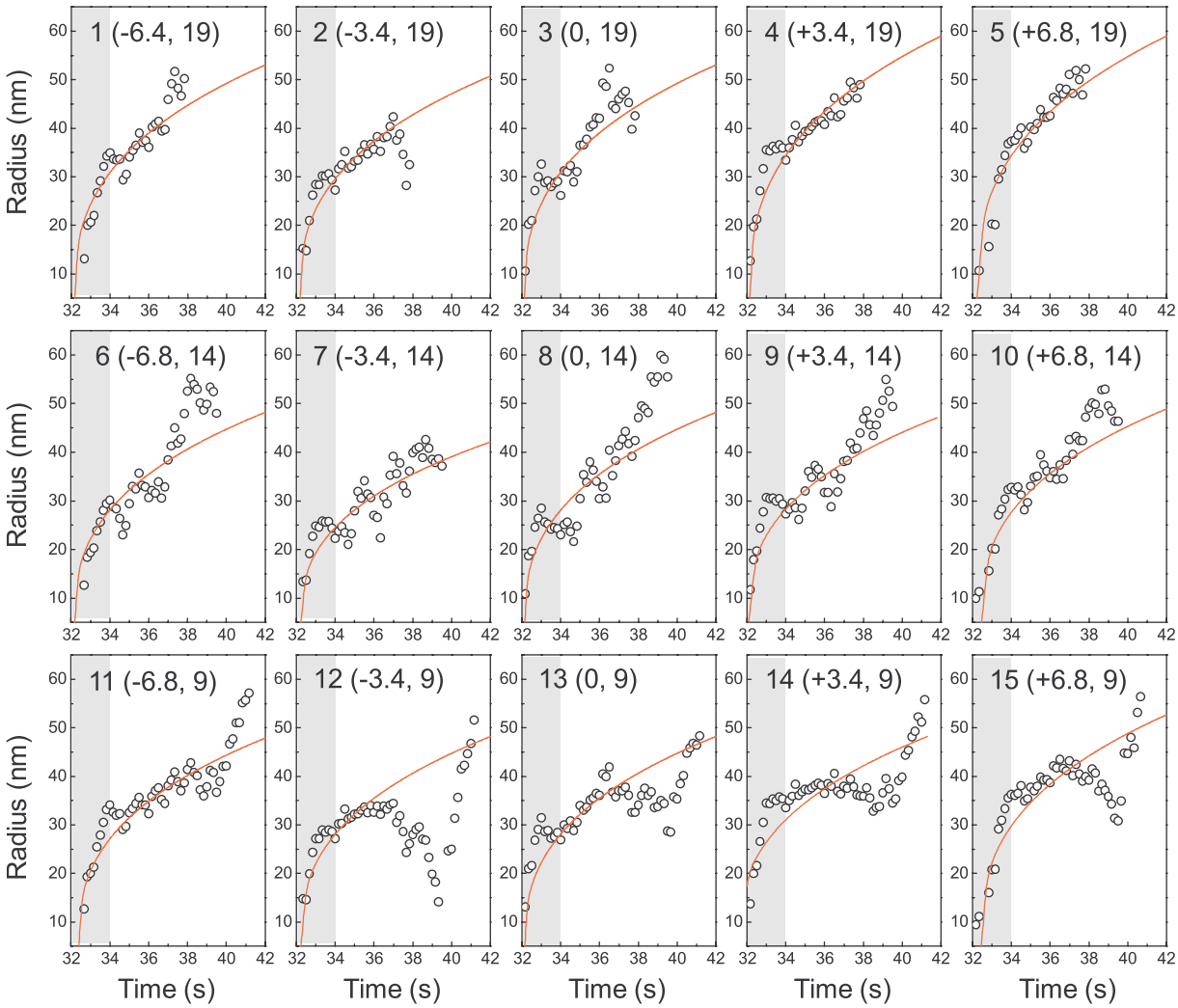

Figure 2. Time evolution of the measured particle radius (circles). Each plot matches with each detection section shown in figure 1(b). The 2D position is designated as (r, z) in millimeters, where (0,0) corresponds to the radial center of the electrode and the electrode surface, respectively. The solid lines indicate the fitted data by the coagulation model.

frame was then divided into five sections in the radial direction as shown in figure 1(b), so that the 15 independent sections were separately analyzed as a function of time.

The plasma source was a typical low pressure capacitively coupled type. The bottom electrode of 12 cm diameter was powered by a 13.56 MHz rf generator (RFPP RF10S) through an impedance matcher. The argon (95%) and silane (5%) mixed gas was injected via a mass flow controller.

3. Experimental results

Figure 2 represents the time evolution of the particle radius in the 2D space at the operating condition of 102 mTorr and 70 W. Each plot matches with each detection section illustrated in

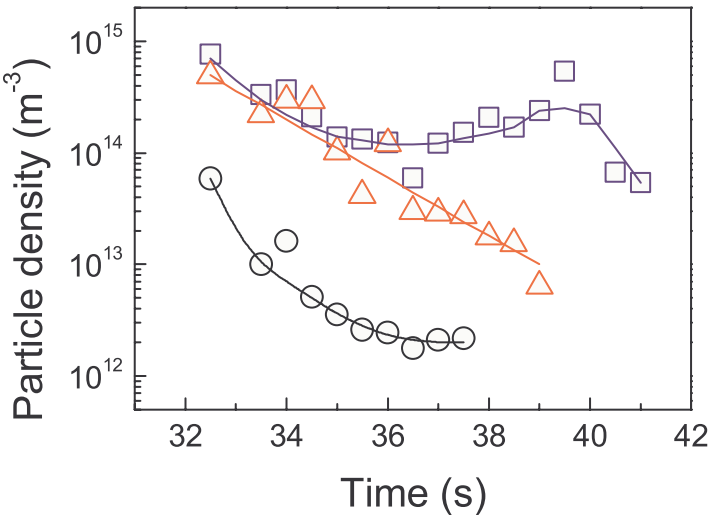

Figure 3. Evolution of the measured particle density at 19 mm (circles), 14 mm (triangles) and 9 mm (squares).

figure 1(b). The 2D position is designated as (r, z) in such a way that (+6.8, 19.0) corresponds to $r = +6.8$ mm and $z = 19$ mm, where $r = 0$ and $z = 0$ indicate the radial center of the electrode and the electrode surface, respectively. In each plot, the abscissa and the ordinate are time and particle radius, respectively. As seen in the plots with open circles, the particle radius overall increases with time. In addition, two different growth periods are observed from the slope of the curves: fast growth period followed by slow growth period. The fast growth period is indicated as the gray region and the rest of the time region is for slow growth with active particle transport. The observed particle growth steps are consistent with already reported papers [3, 6, 9]. The relatively slow particle growth results from the repulsive Coulomb force between the negatively charged particles that hinders the coagulation of the particles with radius of 30–50 nm [12]. After the time $t = 38$ s, the scattered beam starts to disappear due to the formation of the dust-free region at $z = 19$ mm. The dust-free region is further expanded downward ($z = 14$ mm at 40 s, 9 mm at 41 s).

Figure 3 shows the dust particle density obtained by the multi-pass laser extinction method [12] using the measured dust particle radius and the laser extinction ratio. The five multiple laser beam passes were adopted to improve the sensitivity of the measurements. The circles, the triangles and the squares in the figure represent the measured densities at 19, 14 and 9 mm, respectively, and they overall decrease against time, which range from 10^{15} m^{-3} to 10^{12} m^{-3}. The particle density is highest at the lowest vertical position, which is the nearest to the sheath edge.

Figures 4(a) and (b) show the particle growth rates obtained from figure 2 against the vertical position during the fast growth period and the slow growth period, respectively. As seen in the figures, it is shown that the fastest particle growth occurs at $z = 19$ mm, i.e. furthest from the sheath edge in the fast growth period. However, the particle growth rate is more or less similar over the vertical position at the slow growth period.

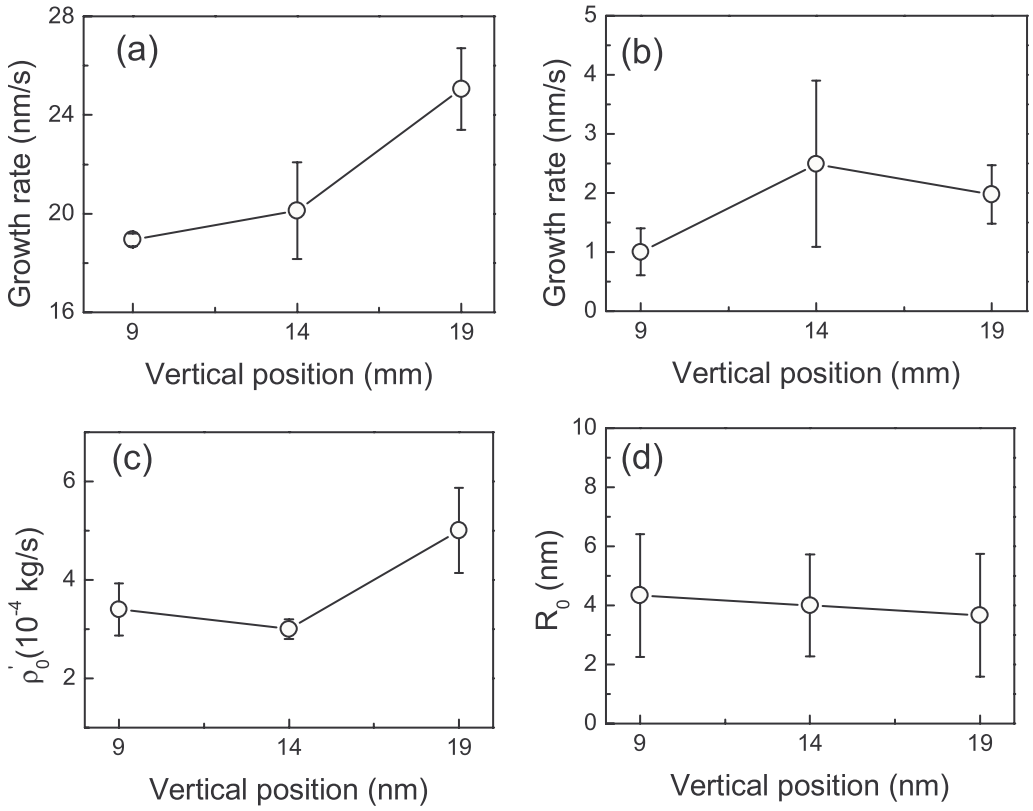

Figure 4. The particle growth rate versus the vertical position during: (a) the fast growth period and (b) the slow growth period. At $z = 19$ mm (furthest from the sheath edge), particles grow faster than at other positions. (c) The proto particle creation rate showing the largest value at $z = 19$ mm. (d) The proto particle radii are about the same in the region under discussion.

4. Discussions

The temporal change of the particle size (figure 2) is compared with the modeling result based on the Lemons coagulation model [13]. Without taking the particle transport into account, it is assumed that predator particles of radius R grow by coagulation of several nm-sized proto (prey) particles of radius R_0. The time derivative of the predator particle radius is expressed as

$$\frac{\mathrm{d}R}{\mathrm{d}t} = \left(\frac{v_{\mathrm{th}}}{4\rho_{\mathrm{d}}}\right)\left[n_{\mathrm{g}}m_0 + \rho_0' t - n_{\mathrm{g}}m_0\left(\frac{R}{R_0}\right)^3\right], \tag{1}$$

where $v_{\mathrm{th}} = (3kT_{\mathrm{d}}/m_0)^{1/2}$ is the thermal speed of the proto particle, m_0 and T_{d} are the proto particle mass and temperature, respectively, ρ_{d} is the proto particle mass density, n_{g} is the constant predator particle number density and ρ_0' is the constant creation rate of the proto particle mass density. Here, it is assumed that $T_{\mathrm{d}} = 1/40$ eV and the dust temperature is not taken into account. The solid curves in figure 2 indicate the modeling result obtained by using R_0 and ρ_0' as fitting parameters that produce the best fit of the measured data. The curves are seen to be in reasonable agreement with the experimental values (circles) until $t \approx 37$ s. The discrepancy may be attributed to the limitation of the Lemons model in which only proto–predator particle

interactions are considered. The scanning electron microscope (SEM) pictures showed some coagulation of the predator particles. As shown in figures 4(c) and (d), where ρ_0' and R_0 versus z are plotted, ρ_0' is larger at $z = 19$ mm than at other vertical positions with the almost same sized (4 nm) proto particles, which means that the fast particle growth is caused by the large proto particle creation rate.

During 38–40 s, the particle radius appears to decrease at $z = 9$ mm (figure 2), and it is believed due to the expansion of the sheath thickness. In the experiment, the thickness of the low optical emission layer above the electrode was about 1 mm during 32–35 s and then gradually increased to 6 mm during 35–40 s. Because the $z = 9$ mm position is nearest to the sheath boundary, the variation of the electric field is largest. Therefore, the particle growth rate appears decreased may be due to the transport of the smaller particles, rather than the actual size reduction of the particles at $z = 9$ mm.

The final data points in time shown in each plot of figure 2 indicate when the dust-free region or the void showed up at each position, which was also confirmed by visual observation of the plasma. At $t = 38$ s, a void forms at $z = 19$ mm. At the same time, there appears a discrepancy between the measured points and the modeling result at $z = 14$ mm. Since the particle sizes are consistent between $z = 19$ and 14 mm at $t = 38$ s, this renders an explanation possible that about 50 nm sized particles trapped at $z = 19$ mm are pushed downward, which eventually become re-trapped at $z = 14$ mm, leading to looking like the larger particle growth rate.

As mentioned above, the dust-free region appeared at around 38 s at $z = 19$ mm ($R \approx$ 50–55 nm) and around 40 s at 14 mm ($R \approx 55$–60 nm), which is caused by the active particle transport. In the plasma, an electric field is established toward the chamber wall because of the large electron mobility. Since the dust particles are negatively charged, the electrostatic force $F_{es} = eZ_pE$ is exerted on the particle toward the bulk plasma, where e is the electron charge. The charge number of the dust particle Z_p is given as [14]

$$Z_p = 0.73\frac{4\pi\varepsilon_0 RkT_e}{e^2}\ln\left[\frac{n_i}{n_e}\left(\frac{m_eT_e}{m_iT_i}\right)^{1/2}\right] \tag{2}$$

for an argon plasma, where R is the dust particle radius, T_e and T_i are the electron and ion temperature, respectively, n_e and n_i are the electron and ion density, respectively, m_e and m_i are the electron mass and the ion mass, respectively, and k is the Boltzmann constant. The electric field E is obtained from the potential $\Phi(z)$ in the pre-sheath region expressed as [15]

$$\Phi(z) = \frac{kT_e}{2}\sqrt{\frac{z-s}{l}}, \tag{3}$$

where s is the vertical position of the sheath edge and l is the bulk plasma scale length. On the other hand, ions are diffused from the bulk plasma to the chamber wall due to the electric field. Therefore, the outward ion drag is exerted on the dust particles, which is given by [16]

$$F_{id} = \pi\, R^2 n_i m_i u_i^2\left(1 - \frac{2\,\mathrm{eV}(R)}{m_iu_i^2}\right) + \frac{\pi}{2}\ln\left(1 + \frac{4}{b^2}\lambda_{DL}^2\right) n_i m_i u_i^2 b^2, \tag{4}$$

where u_i is the ion drift velocity, $V(R)$ is the floating potential of the dust particle, $b = Z_d e^2/2\pi\varepsilon_0 m_i u_i^2$, and λ_{DL} is the linearized Debye length. From the measurement using a floating type probe [17], we got $kT_e = 6.0$ eV and $n_i = 7.0 \times 10^9$ cm^{-3}, and thus the potential and the electric field are calculated to be 0.9 V and 150 V m^{-1}, respectively, at $t = 40$ s and $z = 9$ mm

with $s = 6$ mm and $l = 40$ mm. Using these values, the ion drag force (F_{id}) and the electrostatic force (F_{es}) exerted on the dust particle obtained as a function of particle radius show $F_{id} > F_{es}$ for the particles larger than 54 nm. It means that the particles larger than 54 nm will diffuse out toward the chamber. The particle size is consistent with the measured value of 55–60 nm.

Although the low power laser (30 mW maximum) is used, the 2D LLS method suggested in this work enables measurement of the dust particles as small as 10 nm in radius at the density of 10^{15} m^{-3} (in [9], the detection limit was 25 nm in radius at the density of 10^{15} m^{-3}). Note that the detection limit of our multi-pass LLS method is better than that of the sheet beam LLS.

5. Summary

A temporal evolution of 2D distribution of particle size is shown *in situ* by multi-pass PSLLS in a silane plasma using a relatively simple set-up consisting of a set of spherical mirrors, a low power He–Ne laser, and a 2D CCD detector. The detection limit of our method is 10 nm in radius at the density of 10^{15} m^{-3}. In temporal, the measured data revealed two-step particle growth period and showed a good agreement with the coagulation modeling result. In spatial, the fast particle growth rate was obtained at the furthest from the sheath edge where about 4 nm sized proto particles are abundantly produced. In addition, the particle density is higher at the lower vertical position.

Acknowledgments

This work was partly supported by the Korea Research Foundation grant (KRF-2008–314-C00085) and partly supported by the Korea Science and Engineering Foundation grant (no. R11-2008–072-02001–0) funded by the Korean Government.

References

[1] Selwyn G S, Heidenreich J E and Haller K L 1991 *J. Vac. Sci. Technol.* A **9** 2817
[2] Winter J 2000 *Phys. Plasmas.* **7** 3862
[3] Hollenstein C, Dorier J L, Dutta J, Sansonnens L and Howling A A 1994 *Plasma Sources Sci. Technol.* **3** 278
[4] Shiratani M, Kawasaki H, Fukuzawa T, Yoshioka T, Ueda Y, Singh S and Watanabe Y 1996 *J. Appl. Phys.* **79** 104
[5] Bleecker K D, Bogaerts A and Goedheer W 2006 *New J. Phys.* **8** 178
[6] Seon C R, Choe W, Chai K B, Park H Y and Park S 2009 *New J. Phys.* **11** 013015
[7] Courteille C, Hollenstein C, Dorier J L, Gay P, Schwarzenbach W, Howling A A, Bertran E, Viera G, Martins R and Macarico A 1996 *J. Appl. Phys.* **80** 2069
[8] Bohren C F and Huffman D R 1983 *Absorption and Scattering of Light by Small Particles* (New York: Wiley)
[9] Dorier J L, Hollenstein C and Howling A A 1995 *J. Vac. Sci. Technol.* A **13** 918
[10] Matsuoka Y, Shiratani M, Fukuzawa T, Watanabe Y and Kim K S 1999 *Japan. J. Appl. Phys.* **38** 4557
[11] Childs M A and Gallagher A 2000 *J. Appl. Phys.* **87** 1076
[12] Seon C R, Park H Y, Choe W, Park S and Shin H Y 2007 *Appl. Phys. Lett.* **91** 251502
[13] Lemons D S, Keinigs R K, Winske D and Jones M E 1996 *Appl. Phys. Lett.* **68** 613
[14] Matsoukas T and Russell M 1995 *J. Appl. Phys.* **77** 4285
[15] Oksuz L and Hershkowitz N 2002 *Phys. Rev. Lett.* **89** 145001
[16] Bouchoule A 1999 *Dusty Plasmas—Physics, Chemistry and Technological Impact in Plasma Processing* (New York: Wiley)
[17] Lee M H, Jang S H and Chung C W 2007 *J. Appl. Phys.* **101** 033305